

ACOUSTIC EMISSION ANALYSIS AND SYNCHROTRON-BASED MICROTOMOGRAPHY OF GLUED SHEAR STRENGTH SAMPLES FROM SPRUCE WOOD

Peter NIEMZ¹ Franziska BAENSCH²
Andreas J. BRUNNER³

Abstract: *To better understanding the failure of adhesive joints tensile tests were carried out on miniature test specimens from Norway spruce in the synchrotron. Urea-formaldehyde resin was used as adhesive. e. For comparison purposes, tensile tests were carried out on solid wood and on bonded miniature tensile shear samples with acoustic emission. The acoustic emission signals of all the experiments occurred with classified pattern recognition. This resulted in two classes of signals for each two frequency peaks. One class consisted of the low-frequency and the other of the higher-frequency peak of higher intensity, but this was essentially independent from the structure (solid wood or plywood) and size scale of the test specimens. The influence of the adhesive layers was determined on wood test specimens on laboratory scale and on miniature test specimens with an adhesive layer and selected fiber orientations. This gave evidence that the sound emission signals from the failure of the adhesive layer presumably of the class with low frequency signals peak in the range of services can be assigned.*

Key words: *wood gluing, bondline, in situ test, acoustic emission, synchrotron tomography.*

1. Introduction

The fracture behavior of wooden bonding is determined mainly by the properties of wood (strength, swelling and shrinkage, chemical properties such as extractives), but also by the properties of the pure adhesive

films (e.g., modulus of elasticity, strength).

There are significant differences in the stiffness, and thus in the input of the stresses in the bonded wood among the various adhesive systems [3, 4], [6, 7].

There is also a significant influence of the cutting direction of the wood (l, r, t -

¹ Eidgenössische Technische Hochschule Zürich, Institut für Baustoffe, Zurich, Switzerland;

² Bundesanstalt für Materialforschung und -Prüfung, Berlin, Germany;

³ Eidgenössische Materialprüfungs- und Forschungsanstalt, Dübendorf, Switzerland;

Correspondence: Peter Niemz; e-mail: niemzp@retired.ethz.ch.

direction).

In particular, the differences between wood and glue are considerable parallel to the grain direction. A certain solidification occurs through the bondage perpendicular to the fiber direction [8], [9].

Niemz and Sonderegger [8], specify the following tensile strengths for spruce wood in the fiber direction at 87 MPa, radial at about 4 MPa, and tangential at 3.1 MPa. The modulus of elasticity is 11900 MPa in the l – direction, 817 MPa in the r – direction, and 420 MPa in the t – direction [10]. Stöckel et al. [13], [4] give as example for PUR adhesives an elastic modulus of 500-2000 MPa and for UF adhesive films up to 16000MPa. Wimmer et al. [17] tested sorption properties from different adhesive films.

Work on the strain distribution in bonded wood has been carried so far using digital image correlation or numerical simulation [12].

Wood surfaces also have a significant influence at the microscopic and submicroscopic level. For example, studies on the influence of primers on the strength of bonded joints with AFM have been carried out [2]. Very extensive work has been carried out, in particular, on nano-identification, especially by Konnerth at the Boku in Vienna [11].

In situ measurements in the synchrotron have only been carried out by Baensch [1]. This paper reported on selected

unpublished measurements in the synchrotron from Baensch [1]. The method covers the range between nanoindentation, AFM [11], DIC, and the macroscopic tensile specimens quite well.

2. Material and Methods

The investigation was carried out on bonded wood specimens of miniature size made of clear spruce wood (*Picea abies* (L.) Karst.). Three different specimen types were tested, whereby the geometry of these miniature specimens is similar to that of the miniature specimens made of solid spruce wood. Each specimen type consisted of two wooden layers which were glued together by one single adhesive layer. In all three cases the adhesive layer was oriented parallel to the load direction (shear stresses). The specimen types differ in terms of the fiber-load-angle of the wooden layers. The “LL” specimen consists of two wooden layers oriented with tracheid axes parallel to the load direction (longitudinally).

The “TL” type consists of one longitudinally and one tangentially loaded wooden layer. The “TT” specimen consists of two wooden layers loaded in the tangential direction. For each type, the results are presented by means of selected single specimens.

Table 1

Characterization of tested bonded spruce wood specimens

Sample	Density [kg/m ³]	EMC [%]	Cross section [mm ²]	Speed [mmxs ⁻¹]	Tensile strength [N/mm ²]	Load step	Test duration [min]
LL	471	9.1	1.01	0.010	44	3	60
TL	478	-	1.51	0.010	30	3	49
TT	450	7.9	2.60	0.005	2.68	3	56

The LL specimen was designed to investigate the damage evolution located close to the adhesive layers in the type 6 plywood with two center veneers oriented in the L direction which is also similar to the adhesive-wood connections in the LVL materials (all plies run parallel to each other; loaded in the longitudinal direction).

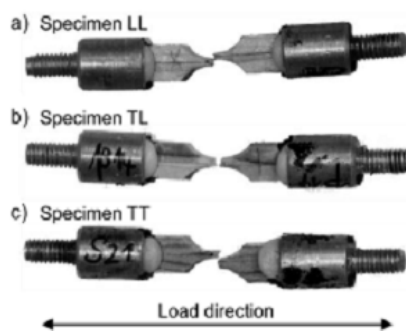


Fig. 1. Photographs of bonded miniature specimens tested under tension: a) LL specimens of two longitudinally oriented wooden layers; b) TL specimen of one longitudinally and one tangentially oriented layer; c) TT specimen of two tangentially oriented wood layers, bonded with urea formaldehyde resin

2.1. Experimental Setup and AE Data Processing

The trials were carried out at the TOMCAT beamline at PSI Villingen. The tensile tests were performed with a loading device (load cell of 1 kN) [15]. The TT specimen was loaded with a cross-head speed of 0.005 mm s⁻¹, and the LL and TL specimens with 0.01 mm s⁻¹. In tomographic monitoring, a digital resolution of 1.62 $\mu\text{m px}^{-1}$ was realized. The AE monitoring was performed with digital AE equipment (AMSY-6, Vallen Systeme GmbH, Icking, Germany), using

two miniature piezoelectric sensors (type M31, Fuji Ceramics Corp. Shizuoka, Japan). For the AE analysis, only the first signal of an AE event detected by both sensors (maximum distance of 10 mm) was evaluated by means of 1D localization. The AE signals were windowed with a Hamming window function and selected frequency 142 features were extracted from the frequency spectra as input parameters to the UPR technique.

3. Results

For each specimen, the unsupervised pattern recognition technique yielded the numerically best separation of the detected AE signals into two clusters. The four main features to identify the similarities between the different waveforms are the peak frequency (PF), the center of gravity frequency (CGF), the weighted peak frequency (WPF), and the partial power 2 (PP2) instead of the partial power 4 (PP4) as conducted for the tested solid wood specimens. However, for comparison purposes, the results are presented with the same set of features as for the latter; PP4 plotted against WPF (Figure 2).

Essentially, two clusters with WPFs of around 300 kHz (A clusters) and 570 kHz (B clusters) were sought out by using the UPR technique. Compared with the A clusters, the B clusters yield a higher contribution from PP2. The former ranges from about 10% to about 80% for all specimen types and the latter from about 0% to 40%. These signal classification results are very similar to those derived from testing solid spruce wood (L and R specimens). In the case of the L and R specimens, the two clusters have tentatively been attributed to inter-wall

cracks (cluster A) and to cell wall cracks in the tracheids (cluster B).

However, the identification of two clusters with comparable WPF ranges and similar amounts of PP4 raises the question of how the layered structure of the bonded miniature specimens with different layup (LL, TL, TT) affects damage behavior compared with solid wood. The plots of PP4 vs. WPF (Figure 2a) clearly reveal that the A cluster forms different patterns of distribution due to the different lay-up systems. For the LL and the LT specimen, the pattern of both clusters A and B equivalent to the R

specimens, the A cluster indicates a possible separation into AE signals with a WPF close to 180 kHz and AE signals close to 330 kHz, though the AE signals with WPFs ranging between 0-400 kHz are found to be associated only with the single A cluster. In the case of the TT specimen, the A cluster could be subdivided into three clusters, since a possible third cluster occurs at 240 kHz. However, these different distribution patterns of the A clusters might be generated by possible different underlying microscopic damage mechanisms due to the lay-up systems loaded.

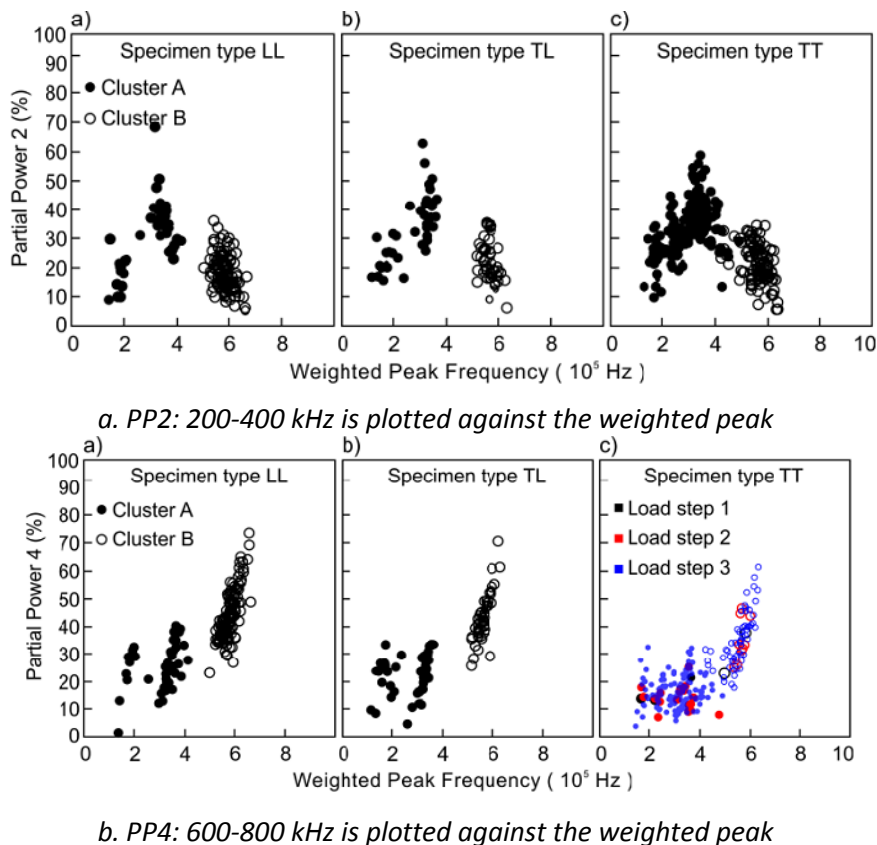


Fig. 2. Cluster formed by pattern recognition of acoustic emission signals (sensors see [1] for bonded wood specimens types and different Partial Power (PP 2 and PP4): a) LL, b) TL, c) TT: Full circles: cluster A, open circles: cluster B, frequency

The appropriate explanation is supported by the results from the SR μ CT scans recorded between the loading steps. The LL specimen (Figure 3), especially the scan taken after the ultimate failure of the specimen (Figures 3a and 3b), shows a crack path mainly running along the growth ring boundary (T direction) and along the grain (R direction), whereby passing the glue line seems to have no impact on the crack path propagation (Figure 3; view of the specimen's test cross section, load direction in the L

direction, perpendicular to R and T). Furthermore, numerous single tracheids fiber bridges were observed. Since UF adhesive provides mechanical properties that are not in the same range as those of spruce when stressed in the L direction, significant weakening or reinforcing effects by the adhesive might be excluded. Instead, the line of least resistance mainly progressed within the two longitudinally loaded wood layers (the load bearing elements in the LL lay-up).

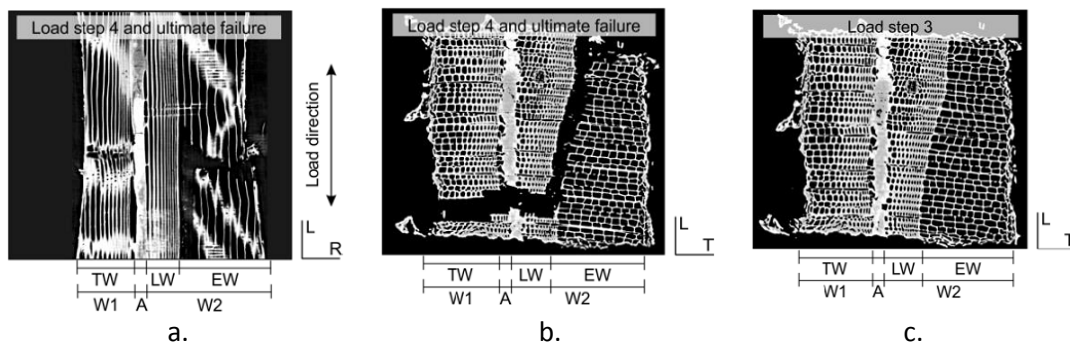


Fig. 3. Fracture pattern of the bonded LL specimen with the view a) parallel and b) perpendicular to load after load step 4. c) The microscopic structure after the previous loading step 3. The position within the specimen is the same in b) and c). Wood layer W1 and W2 bonded together with urea formaldehyde adhesive (A). Early wood (EW), transition wood (TW), and latewood (LW) tissues are distinguished

The same conclusion was derived by means of Environmental Scanning Electron Microscopy (ESEM) images of the fractured cross section, as the complex fracture pattern was formed within both wood layers, whereas the adhesive reveals a smooth fracture surface. However, it has to be pointed out that the bonded miniature specimens tested herein do not provoke the typical tension shear failure, since the wood and the adhesive layers are loaded equally as described by the Hooke springs connected parallel and exposed to pure tension load. In the case

of the TT specimen, the fracture surface of the adhesive looks the same and the wood parts reveal a smooth fracture surface. However, the complexity of its failure behavior is more visible after observation of the tomographic scans taken after each applied load step. In Figure 4 a section of the specimen after the second loading is presented whereby the reconstruction was cut through the glue line to show one half of the specimen with adjacent adhesive. Within the UF adhesive layer, small crack lines induced during hardening are observed (see also [5]).

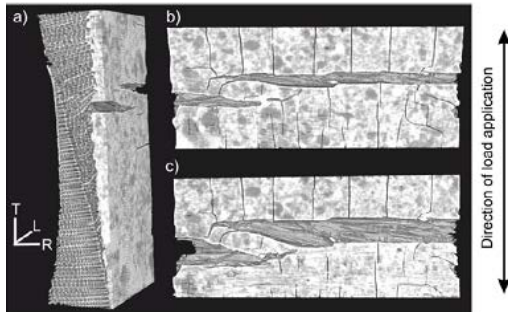


Fig. 4. The crack evolution within the adhesive layer (urea formaldehyde) of the miniature TT specimen is presented by a section of the half specimen. The cut passes the reconstruction through the adhesive layer. Frontal view of the crack opening within the adhesive layer after a) the 2nd and c) the 3rd loading

It seems that crack initiation is located in the adhesive layer and crack lines propagate further parallel to the load direction. After the second loading, significant cracks in the adhesive layer are observed running perpendicular to the load direction, whereby the crack opening also results in displacements within the bordering tracheid tissue. The tracheids are lifted along the T axis, parallel to the direction of the load and crack opening. Cell separation mechanisms and cell wall cracks occur along the RL plane. The comparison of these crack openings after the second and third loading steps gives insight into the relevance of the adhesive within this layup structure of the TT specimen when exposed to tensile load. Another detail selected from the ultimate fracture surface detected immediately after failure shows a tracheid bundle bridge which was pulled out very close to the glue line.

The PP4 vs. WPF plot distinguishes the AE signals with regard to their occurrence

due to the three loading steps applied to the TT specimen (first, second, third step colored black, red, and blue). This reflects the mechanisms of the starting crack (second loading) and of further crack openings (third loading and ultimate failure), as well as the increased consequences for the surrounding tissue in the cluster pattern. However, regarding the three loading steps, no significant trend of occurring cluster positions on the WPF axis is determined. After the first loading step (colored black), few signals of the cluster A already cover the WPFs of 180 kHz to 380 kHz. During the third loading step and the ultimate failure, some AE signals of both cluster A and B show an increased contribution of PP4 (meaning a higher share of high frequency components). However, more tests are needed to verify this tendency.

The analysis of the TL specimen was not continued, since the quality of the SR μ CT scans is unsuitable. Also, the investigation by means of ESEM has proven unsatisfactory due to the couplant for sensor coupling covering the fracture surfaces of the specimen.

3. Conclusions

Similarly, to the miniature tests on solid spruce wood, the acoustic emission signal classification by an unsupervised pattern recognition approach yields two signal clusters for the tensile tests to failure for the bonded miniature specimens for the same levels of partial powers. The clusters essentially differ with respect to higher shares of low and high frequency components. It is assumed that the AE signals generated by the damage mechanisms of the adhesive layer might be covered by the A cluster as discussed

for the LL and TT specimens. The impact of the adhesive layer on the damage evolution of the TT specimen was proven by the reconstructions of the SR μ CT scans, whereas the failure behavior of the LL specimen was mainly dominated by the wooden layers with the tracheid axes oriented parallel to the load direction. This different outcome of the rather brittle UF adhesive is a result of the different grain orientations of the adhered wooden layers. Compared to the UF adhesive, the longitudinally loaded layers have stronger load bearing capabilities, whereas the tangentially loaded wood layers reveal greater weakness. The cluster results plotted as PP4 against WPF prove these observations, since the cluster patterns of the TT specimen show a more individual pattern compared to the solid spruce tested in L and R direction (Figure 2) than the LL specimen. It is assumed that the AE signals generated by the crack mechanisms of the adhesive are among the signals of the low frequency cluster. This tentative conclusion, however, will have to be verified by further investigations, possibly by performing similar tests using other combinations of adhesives and wood species with greater difference in mechanical performance and with a larger number of specimens.

Acknowledgements

The authors acknowledge the financial support of the Swiss National Foundation under grant SNF-Project 177`134.

References

1. Baensch F., 2015. Damage evolution in wood and layered wood composites monitored in situ by acoustic emission, digital image correlation and synchrotron based tomographic microscopy. Zürich: Diss., ETH Zürich.
2. Casdorff K., Kläusler Gabriel J., Amen C. et al., 2018. About the influence of a water-based priming system on the interactions. In: *International Journal of Adhesion and Adhesives*, vol. 80, pp. 52-59.
3. Clauss S., 2011. Structure-property relationships of one-component moisture-curing polyurethane adhesives under thermal load. Zürich: Diss., ETH Zürich.
4. Gindl W., Sretenovic A., Vincenti A. et al., 2005. Direct measurement of strain distribution along a wood bond. Part 2. The Effect of Adhesive penetration on strain distribution. In: *Holzforschung*, vol. 59(3), pp. 307-310.
5. Hass P.F., 2012. Penetration behavior of adhesives into solid wood and micromechanics of the bondline. Zürich: Diss. ETH Zürich.
6. Hering S., 2011. Charakterisierung und Modellierung der Materialeigenschaften von Rotbuchenholz zur Simulation von Holzverklebungen. Zürich: Diss., ETH Zürich.
7. Kläusler O.F., 2014. Improvement of one-component polyurethane bonded wooden joints under wet conditions. Zürich: Diss., ETH Zürich.
8. Niemz P., 2017. Zur Orthotropie der physikalisch-mechanischen Eigenschaften von Fichtenholz. In: *Annals of Warsaw University of Life Science - SGGW. Forestry and Wood Technology*, vol. 99, pp. 174-183.
9. Niemz P., Sonderegger W., 2003. Untersuchungen zur Korrelation ausgewählter Holzeigenschaften

- untereinander und mit der Rohdichte unter Verwendung von 103 Holzarten. In: Schweizerische Zeitschrift für Forstwesen, vol. 154(12), pp. 489-493.
10. Niemz P., Sonderegger W., 2017. Holzphysik-Physik des Holzes und der Holzwerkstoffe. Leipzig: Fachbuchverlag Leipzig im Carl Hanser Verlag.
 11. Rindler A., Pöll C., Hansmann C., 2018. Moisture related elastic and viscoelastic behaviour of wood adhesives by means of in-situ nanoindentation. In: International Journal of Adhesion and Adhesives, vol. 85, pp. 123-129.
 12. Serrano E., 2000. Adhesive joints in timber engineering. Lund: PhD Thesis, Lund University.
 13. Stöckel F., Konnerth J., Gindel-Altmatter W., 2013. Mechanical properties of adhesives for bonding wood - A review. In: International Journal of Adhesion and Adhesives, vol. 45, pp. 32-41.
 14. Wimmer R., Kläusler O., Niemz P., 2013. Water sorption mechanisms of commercial wood adhesive films. In: Wood Science and Technology, vol. 47(4), pp. 763-775.
 15. Zauner M., 2014. In-situ synchrotron based tomographic microscopy of uniaxially loaded wood: in-situ testing device, procedures and experimental investigations. Zürich: Diss. ETH Zürich.